8736 *Inorg. Chem.* **2010**, *49*, 8736–8748
DOI: 10.1021/ic100756f

Inorganic Chemistry
Article

Discrepancies in Thorium Oxide Solubility Values: Study of Attachment/Detachment Processes at the Solid/Solution Interface

Johan Vandenborre,* Bernd Grambow, and Abdessalam Abdelouas

SUBATECH, Unité Mixte de Recherche 6457, École des mines de Nantes, CNRS/IN2P3, Université de Nantes, BP 20722, 44307 Nantes Cedex 3, France

Received April 20, 2010

The solubility of thorium under oxide and/or hydroxide forms has been extensively studied for many years. Nevertheless, a large discrepancy in the solubility values is noticed in the literature. We study Th atom exchange between thorium oxide surfaces and various aqueous solutions (0.01 mol·L^{-1} NaCl for 0.0 < pH < 5.2) to address this issue. By solid-state characterization [X-ray photoelectron spectroscopy (XPS), scanning electron microscopy, and atomic force microscopy], we determined that 80% of the XPS accessible near the surface region of sintered thorium oxide is represented by the less reactive ThO_2(cr) grains. The remaining 20% corresponds to $ThO_x(OH)_y(H_2O)_z$, which is largely associated with grain boundaries. Only the latter fraction is involved in solid/solution exchange mechanisms. Local conditions (thorium concentrations, pH values, etc.) in grain boundaries lead to an adjustment of the "local solubility constraints" and explain the thorium concentration measured in our experiments. For pH <5.2, the thorium concentration and pH gradient between the bulk solution and grain-boundary regions imply that the solubility values mainly depend on the availability and accessibility of $ThO_x(OH)_y(H_2O)_z$. We have performed two solubility experiments with a $^{232}ThO_2$(cr) solid in a 0.01 mol·L^{-1} NaCl solution for 300 days. In a first experiment, we measured ^{232}Th concentrations in dissolution experiments in order to determine the detachment rates of Th atoms from the solid surface. In a subsequent step, we added ^{229}Th to the solution in order to measure the surface attachment rate for dissolved Th atoms. This allowed an assessment of the net balance of Th atom exchange at the solid/solution interface. The empirical solubility data do not correspond to the thermodynamic bulk phase/solution equilibrium because measured solution concentrations are controlled by site-specific exchange mechanisms at the solid/solution interface. Therefore, for sparingly soluble solids, one needs to quantify site-specific surface attachment and detachment rates if one wants to assess solubility constraints.

1. Introduction

The solubility of thorium oxide and/or its hydroxide forms has been studied for many years. The solids are denoted differently in the literature, and there is a lack of thorough solid-state analyses. Typically, X-ray diffraction (XRD) analyses note the "absence of an XRD pattern". This is not sufficient to unambiguously characterize solids. Table 1 presents thorium-based solids used in the various solubility studies in the literature. These studies are grouped in the present work by defining two sets of solids with respect to the crystalline state, the hydroxylation and hydration rate: (1) crystallized thorium oxide synthesized at high temperature with a fully crystalline state as confirmed by XRD analyses [denoted as "ThO_2(cr)"]; (2) thorium hydroxide with hydrous and hydroxyl components ["$ThO_x(OH)_y(H_2O)_z$(am)"]. In the following, various solubility studies are discussed for each group. The results of these solubility studies are reproduced in Figure 1.

1 ThO_2(cr): In most cases for the studies discussed in this group, experimental conditions were not strictly controlled to obtain fully crystallized solids and most of them were not characterized by XRD. The synthesis conditions for obtaining ThO_2(cr) are (1) a slow precipitation with a nitrate or an oxalate precursor and (2) heating at 700 °C for a few days.[1] The solids studied in all works[1−3] were synthesized at high temperature (T = 750 °C) and characterized as fully crystallized solids by XRD. However, the solubility values reported[1,2] in Figure 1, either from an undersaturated experiment (dissolution) using ThO_2(cr) or from oversaturated conditions (precipitation), result in an unidentified, probably amorphous solid. This may explain the observed differences in solubilities. The other solids named ThO_2(cr) are commercially available[4,5] or are sintered sphere fuel for a high-temperature reactor (HTR).[6,7]

*To whom correspondence should be addressed. E-mail: johan.vandenborre@subatech.in2p3.fr. Phone: (+33) 2 51 85 85 36. Fax: (+33) 2 51 85 84 52.

 Published on Web 08/30/2010

Table 1. Data from the Literature about Thorium Oxide Names

publication	name in the paper	solid characterization	name chosen in this work
3	ThO_2(cr)	XRD	ThO_2(cr)
4, 5			
6, 7		XRD	
1, 2			
3, 5, 16, 21−23, 27	ThO_2(microcr)	XRD, BET, electronic diffraction	
9, 27		no	
2, 5, 12, 14, 15, 18−20, 26, 27, 35	ThO_2(coll) or $ThO_n(OH)_{4-2n}\cdot xH_2O$	XRD, electronic diffraction, EXAFS, TEM	$ThO_x(OH)_y(H_2O)_z$(s)
3−5, 8−12, 20, 25, 27	$ThO_2\cdot xH_2O$, ThO_2(am) or $Th(OH)_4$(am)	XRD	

2 $ThO_x(OH)_y(H_2O)_z$(s): This group corresponds not to one solid but to a whole class of different solids. Solid phases in this group are typically obtained by quick precipitation by NaOH addition to an aqueous solution of a nitrate precursor, followed by water washing without heating. In most cases, the experimental synthesis conditions are not detailed in the literature.[3,8−12] Hence, the surface properties are not precisely defined for the obtained solid. Thus, we assume that the studied solids are quite different from one author to another because they depend on the synthesis conditions (precipitation rate, drying time, pH of the media, etc.), as indicated by the review of Rand et al.[13] The amorphous character is often only "identified" by noting the absence of an XRD pattern, but amorphous solids may well be nanocrystalline, as evidenced by electron diffraction. The crystalline/amorphous state was in some cases not studied at all,[9] but there are also detailed studies in which electron diffraction analysis[14,15] and transmission electron microscopy (TEM) techniques have been undertaken. These studies have shown that, for solids precipitated from supersaturated conditions, very small ThO_2(cr) crystallites (1−10 nm) were scattered in an amorphous phase.[16−18] Hence, the notation of "$ThO_x(OH)_y(H_2O)_z$(s)" covers many cases: (a) synthesized solids that are dried for a sufficiently long time (1 week at $T = 25$ °C) to obtain a partial crystallization and that are named "microcrystallized" by the authors;[3,9,16,19−23] (b) other solids that have been precipitated from oversaturated conditions,[14,17,18,24] which show solubility values close to those of colloidal particles measured by laser-induced breakdown detection (LIBD).[4,15,20,25,26]

For some authors,[3,13] the crystallization rate was suggested as an important parameter controlling the solubility of thorium solids. The higher the crystallization rate, the lower the solubility values [cf. $ThO_x(OH)_y(H_2O)_z$(s) data[3] in Figure 1]. Other authors[21,22] have shown that the specific surface area values, measured by Brunauer−Emmett−Teller (BET), strongly depend on the conditions of synthesis of the solid sample ($16\ m^2\cdot g^{-1} <$ surface area $< 76\ m^2\cdot g^{-1}$). At an atomic scale, extended X-ray absorption fine structure (EXAFS) analysis shows that commercial ThO_2(cr) and colloidal particles display different thorium chemical environments.[5] Most authors assume that the solubility properties of the solids are linked to

(1) Hubert, S.; Barthelet, K.; Fourest, B.; Lagarde, G.; Dacheux, N.; Baglan, N., Influence of the precursor and the calcination temperature on the dissolution of thorium dioxide. *J. Nucl. Mater.* **2001**, *297*, (2), 206-213.
(2) Heisbourg, G. Synthèse, caractérisation et études cinétique et thermodynamique de la dissolution de ThO_2 et des solutions solides $Th_{1-x}M_xO_2$ (M = U, Pu). Université Paris XI, Orsay, 2003.
(3) Rai, D.; Moore, D. A.; Oakes, C. S.; Yui, M., Thermodynamic model for the solubility of thorium dioxide in the Na^+-Cl^--OH^--H_2O system at 23°C and 90°C. *Radiochim. Acta* **2000**, *88*, 297-306.
(4) Altmaier, M.; Neck, V.; Fanghänel, T., Solubility and colloid formation of Th(IV) in concentrated NaCl and $MgCl_2$ solution. *Radiochim. Acta* **2004**, *92*, 537-543.
(5) Rothe, J.; Denecke, M. A.; Neck, V.; Müller, R.; Kim, J. I., XAFS investigation of the structure of aqueous Thorium(IV) species, colloids, and solid Thorium(IV) oxide/hydroxide. *Inorg. Chem.* **2002**, *41*, 249-258.
(6) Landesman, C.; Delaunay, S.; Grambow, B., Leaching behavior of unirradiated high temperature reactor (HTR) UO_2-ThO_2 mixed oxides fuel particles. *Mater. Res. Soc. Symp. Proc.* **2004**, 807.
(7) Vandenborre, J.; Abdelouas, A.; Grambow, B., Discrepancies in thorium oxide solubility values: a new experimental approach to improve understanding of oxide surface at solid/solution interface. *Radiochim. Acta* **2008**, *96*, 515-520.
(8) Felmy, A. R.; Rai, D.; Mason, M. J., The solubility of hydrous thorium(IV) oxide in chloride media: development of an aqueous ion-interaction model. *Radiochim. Acta* **1991**, *55*, 177-185.
(9) Moon, H. C., Equilibrium ultrafiltration of hydrolized thorium (IV) solutions. *Bull. Korean Chem. Soc.* **1989**, *10*, (3), 270-272.
(10) Nabivanets, B.; Kudritskaya, L. N., Hydrocomplexes of thorium-(IV). *Ukr. Khim. Zh.* **1964**, *30*, 891-895.
(11) Rai, D.; Felmy, A. R.; Sterner, S. M.; Moore, D. A.; Mason, M. J., The solubility of Th(IV) and U(IV) hydrous oxides in concentrated NaCl anf $MgCl_2$ solutions. *Radiochim. Acta* **1997**, *79*, 239-247.
(12) Ryan, J. L.; Rai, D., Thorium(IV) hydrous oxide solubility. *Inorg. Chem.* **1987**, *26*, (24), 4140-4142.
(13) Rand, M.; Fuger, J.; Neck, V.; Grenthe, I.; Rai, D., *Chemical Thermodynamics of Thorium*. North Holland Elsevier Science Publishers B. V.: Amsterdam, The Netherlands, 2008; Vol. *11*.
(14) Baes, C. F.; Meyer, N. J.; Roberts, C. E., The Hydrolysis of Thorium(IV) at 0 and 95°. *Inorg. Chem.* **1965**, *4*, 518-527.
(15) Bundschuh, T.; Knopp, R.; Müller, R.; Kim, J. I.; Neck, V.; Fanghänel, T., Application of LIBD to the determination of the solubility product of thorium (IV)-colloids. *Radiochim. Acta* **2000**, *88*, 625-629.
(16) Dzimitrowicz, D. J.; Wiseman, P. J.; Cherns, D., An electron microscope study of hydrous thorium dioxide $ThO_2.nH_2O$. *J. Colloid Interface Sci.* **1985**, *103*, (1), 170-177.
(17) Rousseau, G.; Fattahi, M.; Grambow, B.; Boucher, F.; Ouvrard, G., Coprecipitation of thorium with UO_2. *Radiochim. Acta* **2002**, *90*, (9), 523-527.
(18) Rousseau, G.; Fattahi, M.; Grambow, B.; Boucher, F.; Ouvrard, G., Coprecipitation of thorium and lanthanum with UO_{2+x}(s) as host phase. *Radiochim. Acta* **2006**, *94*, 517-522.
(19) Jernström, J.; Vuorinen, U.; Hakanen, M. *Solubility of thorium in 0.1 M NaCl solution and in saline and fresh anoxic reference groundwater*; **2002**.
(20) Neck, V.; Müller, R.; Bouby, M.; Altmaier, M.; Rothe, J.; Denecke, M. A.; Kim, J. I., Solubility of amorphous Th(IV) hydroxide - application of LIBD to determine the solubility product and EXAFS for aqueous speciation. *Radiochim. Acta* **2002**, *90*, 485-494.
(21) Östhols, E., The solubility of microcrystalline ThO_2 in phosphate media. *Radiochim. Acta* **1995**, *788*, 1-6.
(22) Östhols, E.; Bruno, J.; Grenthe, I., On the influence of carbonate on mineral dissolution: III. The solubility of microcrystalline ThO_2 in CO_2-H_2O media. *Geochim. Cosmochim. Acta* **1994**, *58*, (2), 613-623.
(23) Wierczinski, B.; Helfer, S.; Ochs, M.; Skarnemark, G., Solubility measurements and sorption studies of thorium in cement pore water. *J. Alloys Compd.* **1998**, *271−273*, 272-276.
(24) Heisbourg, G.; Hubert, S.; Dacheux, N.; Ritt, J., The kinetics of dissolution of $Th_{1-x}U_xO_2$ solid solutions in nitric media. *J. Nucl. Mater.* **2003**, *321*, (2−3), 141-151.
(25) Altmaier, M.; Neck, V.; Müller, R.; Fanghänel, T., Solubility of $ThO_2.xH_2O$(am) in carbonate solution and the formation of ternary Th(IV) hydroxide-carbonate complexes. *Radiochim. Acta* **2005**, *93*, (2), 83-92.
(26) Bitea, C.; Müller, R.; Neck, V.; Walther, C.; Kim, J. I., Study of the generation and stability of thorium(IV) colloids by LIBD combined with ultrafiltration. *Colloids Surf., A* **2003**, *217*, (1−3), 63-70.
(27) Neck, V.; Kim, J. I., Solubility and hydrolysis of tetravalent actinides. *Radiochim. Acta* **2001**, *9*, 1-16.

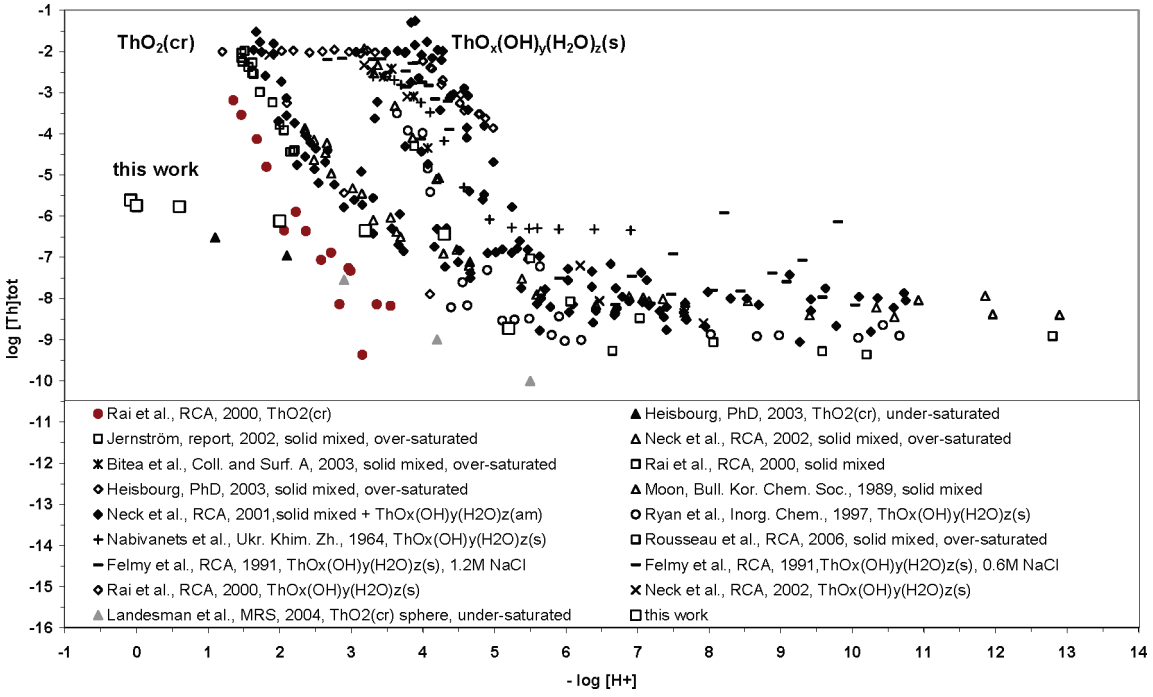

Figure 1. Solubility values from the literature and the present work.

surface phenomena.[8,13,27] A recently published work[13] sheds some light on the difficulty in performing realistic solubility experiments with ThO_2. They indicate that many authors have spent insufficient effort in separating the solid and aqueous phases. Measured thorium concentrations were often higher because colloidal particles and/or polynuclear species were not sufficiently filtrated. The authors[13] underline that the solubility is not controlled by the solid bulk but rather by amorphous or unidentified microcrystalline surface phases. Moreover, they notice that the published studies have been carried out using thorium hydroxide phases within a large range of particle sizes, caused by variation of the synthesis conditions and aging times. Using four sets of particle sizes [>30, 10−30, 5−10, and <5 nm (measuring by an independent method)] and by determining the surface energy contributions to the solubility, they propose an explanation for the discrepancy in the thorium solubility values. The work presented here tries to bring to a whole this point of view.

To conclude, Figure 1 shows that three sets of solubility values are linked to two kinds of solids: (1) solid $ThO_x(OH)_y(H_2O)_z(s)$ with high solubility values (1×10^{-2} mol·L^{-1} for pH 4.5); (2) solid ThO_2(cr) with low solubility values (1×10^{-7} mol·L^{-1} for pH 2.5); (3) a solid that is not clearly identified with a broad range of intermediate solubility values (between 1×10^{-2} and 1×10^{-6} mol·L^{-1} for pH 3.5). The corresponding variation in the solubility products is presented in Table 2, using, for both solids, the formal stoichiometric reaction

$$ThO_2 + 2H_2O \leftrightarrow Th^{4+} + 4OH^- \quad (1)$$

The solubility product values range between ThO_2(cr) ($\log K°_{sp} = -56.9$[3]) and $ThO_x(OH)_y(H_2O)_z(s)$ ($\log K°_{sp} = -45.5$[8,11]), while an average value was suggested for the amorphous phase[26] ($\log K°_{sp} = -47$). Moreover, a difference has been established[11] between freshly prepared hydroxide ($\log K°_{sp} = -46.7$) and the aged phase ($\log K°_{sp} = -47.5$). A solubility product has been calculated from thermodynamic data, derived from calorimetric experiments ($\log K°_{sp} = -54.2$[28−30]) for ThO_2(cr). However, authors[13] have suggested that the formation of OH groups on the surface modifies the solubility of ThO_2(cr) when compared to the solubility values calculated from microcalorimetric measurements. However, most oxides, like, for example, SiO_2, form OH groups at the surface, but this does not lead to the discrepancy between solid-state thermodynamic data and thermodynamic data obtained from the solubility values. Hence, despite the careful recent review of thermodynamic data,[13] it is still not clear how to predict the thorium oxide solubility. Hence, the large uncertainty in the solid-phase properties and solubility product values demands a new approach linking the bulk solid, solid surface, and solubility properties. We use solid analysis,

Table 2. Solubility Product Values from the Literature

solid	$\log K°_{sp}$ (exptl)	publication
$ThO_x(OH)_y(H_2O)_z(s)$	−53.2	5
	−49.2	3
	−52.8	15
	−48.7	22
	−47	27
	−52.9	9, 20
	−47.8	20
	−46.6	9
	−45.5	8
	−45.5	11
	−47.3	12
	−46.6	10, 14
	−46.2	3
ThO_2(cr)	−56.9	3

(28) Cox, J. D.; Wagman, D. D.; Medvedev, V. A., *CODATA Key Values for Thermodynamics*. Hemisphere Pub. Corp.: 1989; p 271.
(29) Fuger, J.; Oetting, F. L., *The Chemical Thermodynamics of Actinide Elements and Compounds: Part 2, The Actinide Aqueous Ions*. Vienna, 1976.
(30) Wagman, D. D.; Evans, W. H.; Parker, V. B.; Schumm, R. H.; Halow, I.; Bailey, S. M.; Churney, K. L.; Nuttal, R. L., The NBS Tables of Chemical Thermodynamic Properties, Selected Values for Inorganic and C_2 Organic Substances in SI Units. *J. Phys. Chem.* **1982**, *11*, (2).

Table 3. Properties of the ThO_2(cr) Solid Used in the Present Work

sphere	ThO_2(cr)
diameter (mm)	0.5
weight (mg)	0.69
density ($g \cdot cm^{-3}$)	10.00
specific area ($m^2 \cdot g^{-1}$)	1.2×10^{-3}
area for one sphere (m^2)	0.8×10^{-6}

a leaching experiment, and isotopic exchange to contribute to the understanding of the discrepancy in the solubility data and to describe the degree of reversibility in exchange mechanisms.

2. Experimental Section

The solid used in this study was provided by J. Fachinger from Forschungzentrum Jülich (Germany). The particles were spherical and synthesized at a high calcination temperature (1600 °C). The synthesis method is described elsewhere.[31] Table 3 presents the properties of the solid studied. Solid analysis was performed by atomic force microscopy (AFM), scanning electron microscopy (SEM), and X-ray photoelectron spectroscopy (XPS) techniques.

The O_{1s} and $Th_{4f_{7/2-5/2}}$ XPS spectra were collected by an XPS apparatus (Leybold) with a Leybold LHS12 electron spectrometer working in fixed analyzer transmission mode. The source of photons was a magnesium anode X-ray source emitting Mg $K\alpha_{1,2}$ radiation producing an incident X-ray beam at 1253.6 eV with a full-width at half-maximum (fwhm) of 0.70 eV. The sample, fixed on a metallic plate, was analyzed in a chamber under 5×10^{-7} Pa vacuum. The O_{1s} and $Th_{4f_{7/2-5/2}}$ peaks were recorded at a constant pass energy of 31.5 eV. Because of the poor electrical conductivity of this oxide, the charge effects were corrected using the C_{1s} line of the carbon at 284.7 eV. The angle-resolved XPS spectra were fitted with the *XPSPeak4.1* program,[32] using a Gaussian−Lorentzian peak shape with a Shirley baseline as the background. The binding energy precision was about 0.3 eV.

The SEM microscope used in this work is a JEOL 5800 SV with a 15 kV voltage. The SEM samples were covered by a platinum layer in order to improve the electron conduction and increase the picture resolution. The AFM pictures were obtained by a Digital Instruments Dimension 3100, Nanoscope V, apparatus.

Batch experiments were performed by exposing 150 spheres of $^{232}ThO_2$(cr) to an aqueous solution at undersaturated conditions. A high-density polyethylene (HDPE) reaction vessel, containing 15 mL of a 0.01 $mol \cdot L^{-1}$ NaCl solution under continuous agitation, was used. The pH was varied between 0 and 5.2 by the addition of small aliquots of 0.1 $mol \cdot L^{-1}$ HCl, as presented in Table 4. Either initially (series I; Table 5) or in a second step after 133 days (series II), solutions were spiked with a ^{229}Th ($t_{1/2}$ = 7340 years) carrier-free solution to achieve a final $[^{229}Th]_{aq} = 4.9 \times 10^{-10}$ $mol \cdot L^{-1}$. The addition date of 133 days corresponds to the time necessary to reach a constant ^{232}Th concentration ("steady state"). Immediately after the addition of the acid ^{229}Th aliquot, the acid perturbation of the solution pH was compensated for by the addition of small aliquots of 0.01 $mol \cdot L^{-1}$ NaOH until the target pH values were reached again. The objective of adding the spike is to test the reversibility and to allow one to follow the potentially ongoing solution/surface isotopic exchange on the ThO_2(cr) surface at "steady state". The dissolution process of $^{232}ThO_2$(cr) and the uptake of ^{229}Th from solution are monitored by sampling aliquots of 0.5 mL over a period of 320 days. Solution samples were ultrafiltered, using 1.8 nm cutoff membranes (5 kDa) in order to exclude colloidal particles commonly described in the literature.[4,20,26,27] The ultrafiltered solutions were then acidified and analyzed by inductively coupled plasma mass spectrometry (ICP-MS) for determination of the ^{232}Th concentration in solution ($[^{232}Th]_{aq}$) with an estimated error of ±10%. Aliquots of the spiked solutions were measured directly in the same ultrafiltered solutions using α spectrometry (error ±20%, E_α = 4.845 MeV) after deposition of a solution aliquot on a stainless steel counting plate and calcination at 500 °C for 12 h.

Table 4. Experimental Conditions of Batch Leaching (Dissolution) Experiments

parameter	value
temperature (°C)	23
S/V (m^{-1})	8
pH	0/0.6/2.0/3.2/4.3/5.2
contact time (days)	320

Table 5. Notation of Experiments Conducted in This Work: Series I (*xx*-I) Corresponds to Experiments with the Addition of a Radiotracer at t = 0 and Series II (*xx*-II) to Those with Addition after 133 days, *xx* = pH

	^{229}Th add in	
pH	t = 0 days	t = 133 days
0.0	00-I	00-II
0.6	06-I	06-II
2.0	20-I	20-II
3.2	32-I	32-II

An additional blank experiment was performed in parallel using the same experimental conditions but without the presence of the solid phase. These experiments confirmed that the spike addition procedure does not imply local thorium precipitation by pH adjustment. In addition, the experiments without ThO_2(cr) spheres but with ^{229}Th show no sorption on the container walls. We also note that, for experiments with ThO_2(cr) particles at pH 4.3 and 5.2, ^{229}Th could not be measured by α spectrometry because activities were below the detection limit.

3. Data Treatment

3.1. Normalization of Solution Concentrations and Rate Values. The measured solution concentrations in leaching experiments are normalized to the solid composition and surface area and expressed as normalized mass loss NL using the equation

$$NL = \frac{[Th]MW_{ThO_2}}{S/V} \quad (2)$$

where [Th] signifies the measured ^{232}Th concentrations in $mol \cdot m^{-3}{}_{H_2O}$, MW_{ThO_2} is the molecular weight of ThO_2 ($g \cdot mol^{-1}$), S is the surface area (m^2) of the solid, and V is the solution volume (m^3). The geometrical surface area of the spheres is used for S as the reference because S is too low to be measured by the gas adsorption method. In many cases, the geometric surface area estimations of ceramics are good estimates of the experimental values.[33] The normalized dissolution rate (in $g \cdot m^{-2} \cdot day^{-1}$) is then calculated with the following equation:

$$NLR = \frac{\Delta NL}{\Delta t} \quad (3)$$

(31) Müller, A., Establishment of the technology to manufacture uranium dioxide kernels for PBMR fuel. *Proceedings HTR2006: 3rd International Topical Meeting on High Temperature Reactor Technology* **2006**, B00000070.

(32) Kwok, R. W. M. *XPSPeak95, 4.1*; The Chinese University of Hong Kong: 1999.

(33) Alliot, C.; Grambow, B.; Landesman, C., Leaching behaviour of unirradiated high temperature reactor (HTR) UO_2-ThO_2 mixed oxides fuel particles. *J. Nucl. Mater.* **2005**, *346*, (1), 32-39.

where Δt signifies an interval in the contact time (days) and ΔNL variation of the normalized mass loss in this interval.

3.2. Isotopic Exchange Data. The relationship between the dissolution and precipitation rates coupled to isotopic exchange data is given in eq 4. For simplification, we use an equation valid for the neutral to alkaline pH range, where $Th(OH)_4$ is the dominant solution species. In acid, there are other solution species to be considered, but the reactions are similar.

Assuming a constant rate of $\vec{r}$ surface-site detachment (constant forward rate of dissolution), we obtain with the surface area S a surface area normalized forward rate constant $\vec{k}$:

$$^{232}ThO_2(s) \xrightarrow{H_2O} {}^{232}Th(OH)_4(aq)$$
$$\text{rate } \vec{r} = \vec{k} \cdot S \tag{4}$$

This rate is not to be confused with that given in eq 3, which is the overall rate, not the forward dissolution rate described here. If we now assume that all surface sites have an equal probability of detachment, we can formulate, from the total trace quantity of ^{229}Th adsorbed on the surface, the rate of isotopic detachment:

$$^{229}Th(s) \rightarrow {}^{229}Th(aq)$$
$$\text{rate } {}^{229}\vec{r} = \vec{k} \cdot S \left(\frac{^{229}Th}{^{232}Th}\right)_{surface} \tag{5}$$

However, because isotopic surface coverage is a function of the time until isotopic exchange equilibrium, the isotopic detachment rate is, in general, not constant with time.

Similarly for ^{232}Th, we can formulate an attachment rate that depends on the solution concentration of ^{232}Th:

$$^{232}Th(OH)_4(aq) \xrightarrow{-H_2O} {}^{232}ThO_2(s) \tag{6}$$
$$\text{rate } \overleftarrow{r} = \overleftarrow{k} \cdot S[^{232}Th(OH)_4(aq)]$$

The equation for isotopic attachment is similar:

$$^{229}Th(aq) \rightarrow {}^{229}Th(s)$$
$$\text{rate } {}^{229}\overleftarrow{r} = \overleftarrow{k} \cdot S[^{229}Th(aq)] \tag{7}$$

At chemical equilibrium:

$$\vec{r} = \overleftarrow{r} \Rightarrow \vec{k} = \overleftarrow{k} \cdot [Th(OH)_4(aq)]_{eq}$$
$$\Rightarrow K_{sp} = \frac{\vec{k}}{\overleftarrow{k}} = [Th(OH)_4(aq)]_{eq} \tag{8}$$

At isotopic exchange equilibrium:

$$^{229}\vec{r} = {}^{229}\overleftarrow{r} \Rightarrow \vec{k} \cdot \left(\frac{^{229}Th_{eq}}{^{232}Th}\right)_{surface}$$
$$= \overleftarrow{k} \cdot [^{229}Th(aq)]_{eq} \Rightarrow K_{sp} = \frac{\vec{k}}{\overleftarrow{k}} = \frac{[^{229}Th(aq)]_{eq}}{\left(\frac{^{229}Th_{eq}}{^{232}Th}\right)_{surface}} \tag{9}$$

However, this latter reaction can only be applied if the quantity of ^{232}Th participating in the isotopic exchange at the surface is known. If all Th atoms at the surface participate in the exchange, one would be able to calculate the concentration of thorium at the surface simply from the crystallographic site density. In that case, at isotopic equilibrium, the isotopic composition at the surface should equal the isotopic concentration in solution and one should be able to use eq 9 to obtain solubility data. In a more general case, the concentration of exchanging Th atoms at the surface might be larger or smaller than the crystallographic site density, smaller if a certain number of surface sites is nonreactive and larger if there is a second phase (for example, a surface precipitate) containing thorium at a higher specific surface area. Thus, we can use eq 9 together with the measured K_{sp} of ^{232}Th to calculate the number of Th atoms at the surface interacting with the solution:

$$\frac{^{232}Th_{exchange}}{^{232}Th_{crystallographic}} = \frac{K_{sp,\,measured}}{K_{sp,\,crystallographic}} \tag{10}$$

where $K_{sp,crystallographic}$ is the K_{sp} value determined from isotopic exchange assuming that all surface sites participate in the exchange. This ratio also corresponds to the ratio of the isotopic ratios at the surface relative to that in solution assuming thorium concentrations at crystallographic site densities or to the relative enrichment/depletion of ^{229}Th at the surface.

Equation 10 can only be used to quantify the exchangeable thorium at the surface if it is assured that all ^{229}Th is exchangeable, i.e., when the isotopic equilibrium is independent of the time of the experiment (once solubility equilibrium is attained) and independent of the time of the addition of ^{229}Th. The fraction of irreversibly fixed ^{229}Th can be estimated from the following isotopic exchange equilibrium as a function of time.

4. Results

4.1. Solids Analysis. Two solids are analyzed by SEM, AFM, and XPS: one called "blank", designating the solid before the leaching experiment, and the second called "leached pH 3.2", designating the solid that was removed after 120 days from the 0.01 $mol \cdot L^{-1}$ NaCl solution at pH = 3.2.

The SEM analysis shows that the solid surface is constituted of grains and grain boundaries (cf. Figure 2, picture "blank"). The grain sizes range between 2 and 0.5 μm. Only Th and O atoms are detected by energy-dispersive X-ray analyses. On the "leached pH 3.2" micrograph, it is seen that the grain boundaries have been subjected to severe leaching.

In order to quantify dissolution of the solid at grain boundaries, a more detailed study of the surface morphology is conducted using AFM. Results obtained are consistent with the SEM data (leaching of grain boundaries). Also, pullout of a few grains is observed. A leaching depth of 50 nm is observed in the grain boundaries (Figure 3). By AFM, the average grain size is determined to be 1 μm in the xy plane. From grain pullout, we obtain a single value for the grain thickness of about 300 nm in the z direction.

Additional XPS analyses, with the initial (blank) and leached solid, are conducted at pH 3.2, 4.3, and 5.2. The depth analyzed by this technique is 3 nm. Table 6 gives parameters used in order to fit XPS spectra of $Th_{4f_{7/2-5/2}}$ and O_{1s}.

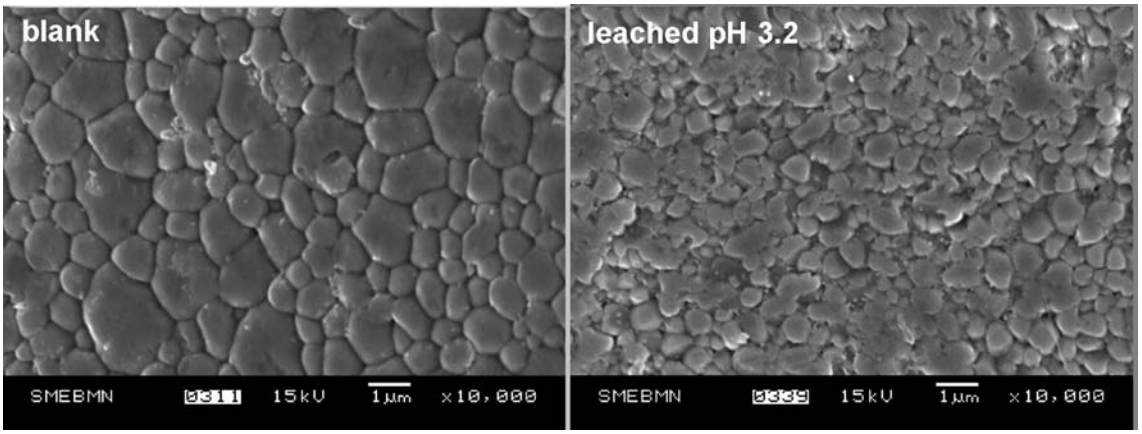

Figure 2. SEM pictures for two samples of the ThO_2(cr) studied solid.

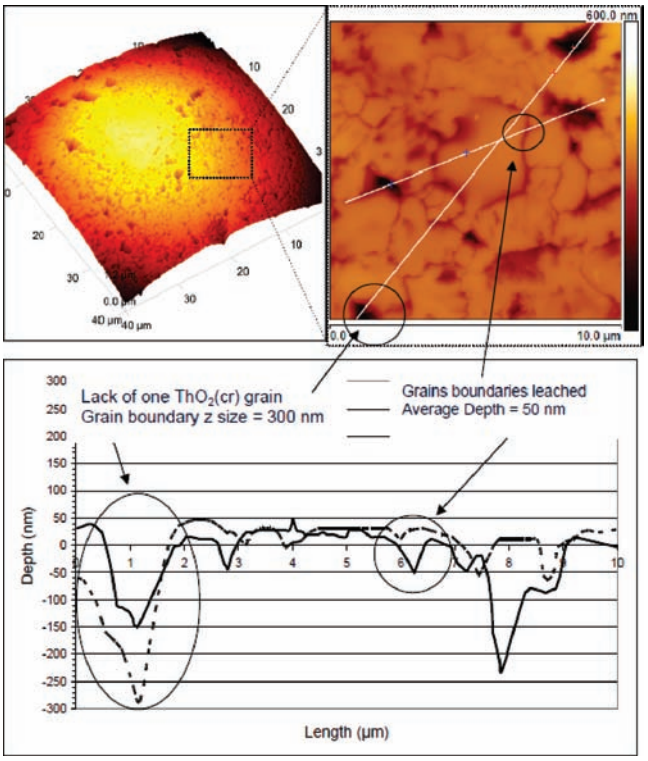

Figure 3. 2D and 3D AFM pictures and a measured profile of the "leached pH 3.2" sample.

Figure 4 presents XPS spectra for the two samples: blank and "leached pH 3.2". Before leaching, two chemical environments of thorium are present at the solid surface: for $Th_{4f_{7/2}}$, the first peak with the higher area at BE = 333.9 eV is named "Th(1)" and the second peak with the lower area at BE = 337.1 eV is named "Th(2)". The same difference (ΔBE = 337.1−333.9 = 346.4−343.2 = 3.2 eV) is found for the $Th_{4f_{5/2}}$ peaks. The area ratio between Th(1) and Th(2) indicates that Th(1) accounts for 81% of the total observed thorium and Th(2) for 19%. Concerning the O_{1s} spectrum, three components are present: O^{2-} (36%), OH (47%), and OH_2 (17%). Thus, the solid at the surface consists of a mixture of oxide and hydrated phases.

For the solid leached at pH 3.2, the $Th_{4f_{7/2-5/2}}$ spectrum shows the disappearance of the peaks associated with Th(2), suggesting that dissolution of this component controls the

Table 6. Parameters Used in Order To Fit XPS Spectra

spectra	peak	BE (eV)	fwhm (eV)	Lorentzian/Gaussian ratio (%)
O_{1s}	O^{2-}	529.7	1.7	60
	OH	532.0	1.7	60
	OH_2	533.7	2.3	60
$Th_{4f_{7/2-5/2}}$	$Th_{4f_{7/2}}$(1)	333.9	1.6	70
	$Th_{4f_{7/2}}$(2)	337.1	1.8	70
	satellite	341.1	1.7	70
	$Th_{4f_{5/2}}$(1)	343.2	1.6	70
	$Th_{4f_{5/2}}$(2)	346.4	1.8	70

observed solution concentrations of thorium. For the O_{1s} spectrum, the OH_2 component disappears completely and the OH peak area decreases by about one-third. Thus, without being able to conclude from the XPS data on the potential mobilization of Th(1), one can conclude that the leaching process resulted in the complete dissolution of a phase composed of 19% of the thorium present in the Th(2) form, 17% of oxygen in the form of OH_2, and 16% (=47/3%) of oxygen in the OH form. Hence, we conclude that Th(1) corresponds to the Th atom in the ThO_2(cr) bulk grain matrix and the more leachable surface region is characterized by the compositional features of Th(2), which is also the principal form of thorium in the vicinity of grain boundaries. This phase with hydroxyl and hydrous parts can be named "$ThO_x(OH)_y(H_2O)_z$".

The results with samples leached at pH 4.3 and 5.2 are similar to those described above with the sample leached at pH 3.2. For pH 5.2, XPS analyses do not show any new chemical environments on the $Th_{4f_{7/2-5/2}}$ spectrum, thus excluding new phase precipitation of an extent that would have allowed detection by XPS.

4.2. Solution Analyses. Figure 5 shows [^{232}Th] with respect to the contact time for each pH value. Two domains can be seen: the first one is for a contact time between 0 and 50 days (domain I) with a higher leaching rate; the second one is for a contact time beyond 50 days (domain II) with either a lower leaching rate or an approach to steady-state concentration values. The final steady-state [^{232}Th] values measured in our system are presented in Table 7 for a contact time of 120 days together with the normalized leaching rate (NLR) for the two domains. A third domain is noticed but not shown in this paper and concerns ^{232}Th precipitation during the addition of ^{229}Th. This can be explained by a nucleation/precipitation effect.

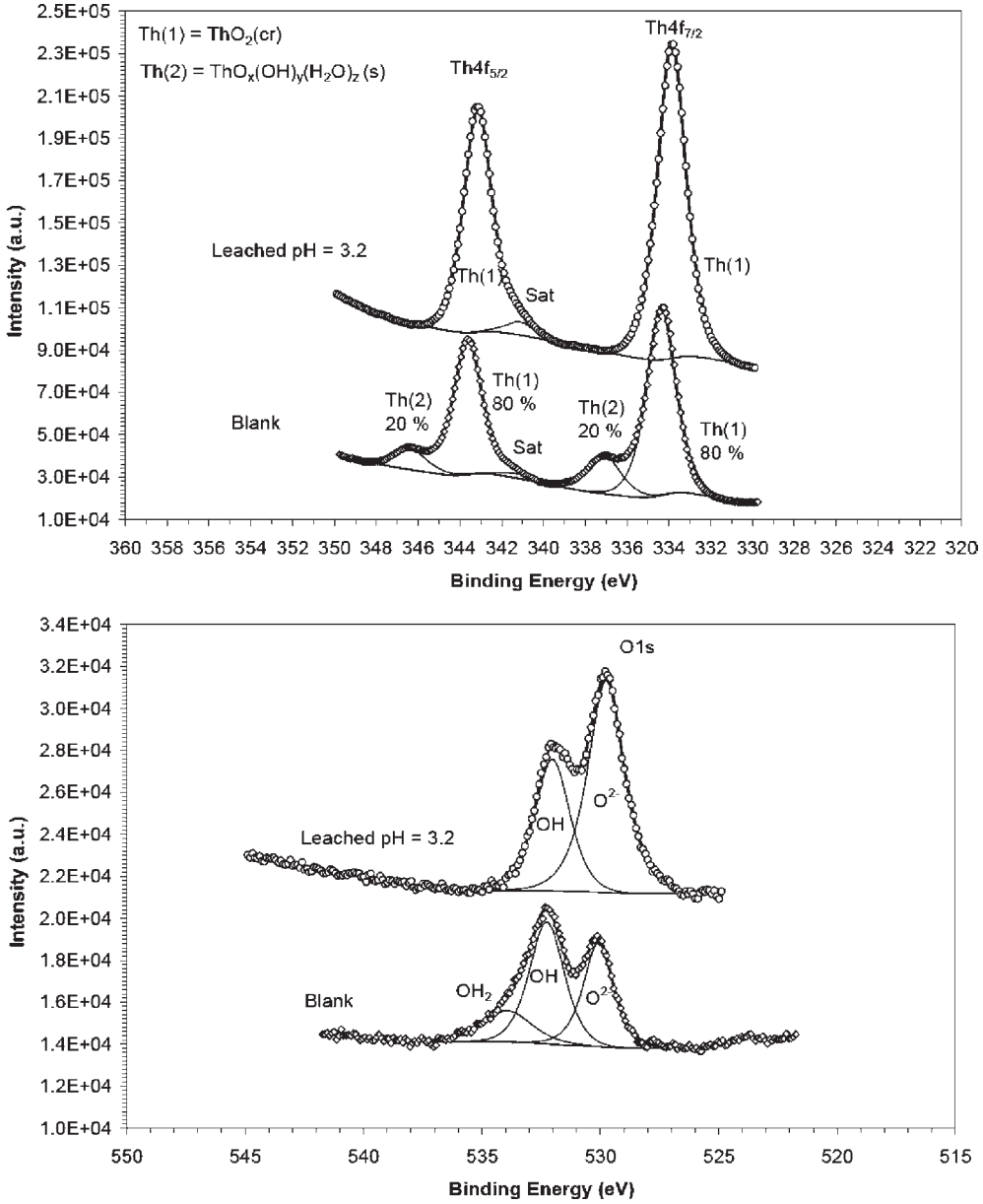

Figure 4. XPS spectra of $Th_{4f_{7/2-5/2}}$ and O_{1s} for the blank and leached samples.

The rate values for domain II have very large uncertainties and for pH >0.6 cover only the period of approach of steady-state concentrations. The measured final steady-state concentrations (domain II) are plotted in Figure 1 in comparison to the solubility data from the literature. In our experiments at pH ≤ 3.2, [^{232}Th] values measured are orders of magnitude lower than most reported solubility values. Only a few data[1,2] observed during the undersaturated experiments are similar to ours. In this experiment, the thermodynamic equilibrium of solubility is not achieved with a solid composed by grains and grain boundaries. A comparison of our dissolution rates (domain I and initial domain II) with the literature data is given in Figure 6. Despite ^{232}Th solution concentrations similar to literature values,[1,2] we observe much higher NLR values.

4.3. ^{229}Th/^{232}Th Exchange Data. Figure 7 presents, as an example, evolution of [^{232}Th] and [^{229}Th] with respect to the contact time for the sample leached at pH 3.2. Upon the addition of the spike of ^{229}Th to series II experiments (the addition after reaching a steady state after 122 days), the ^{232}Th concentrations first decrease sharply and then increase again over a period of 150 days almost to their values prior to the ^{229}Th addition, while the concentrations of ^{229}Th decrease at the same time. Hence, initially some precipitation of ^{232}Th must have occurred followed by rapid redissolution, a process probably due to some chemical perturbation imposed during spike addition. At the same time, an exchange between ^{232}Th atoms on the solid surface and ^{229}Th atoms in the aqueous solution occurs. In other words, there exists a dynamics of dissolution and precipitation reactions and/or of detachment/attachment rates.

Table 8 shows the results of [^{229}Th] measured by α spectrometry for an aliquot of each sample at 0, 133, and 300 days. It is reminded that two kinds of experiments were performed with a ^{229}Th addition at either 0 or 133 days (cf. Table 5). For each sample, we can see that the ^{229}Th concentration has decreased, indicating the attachment of ^{229}Th to the solid

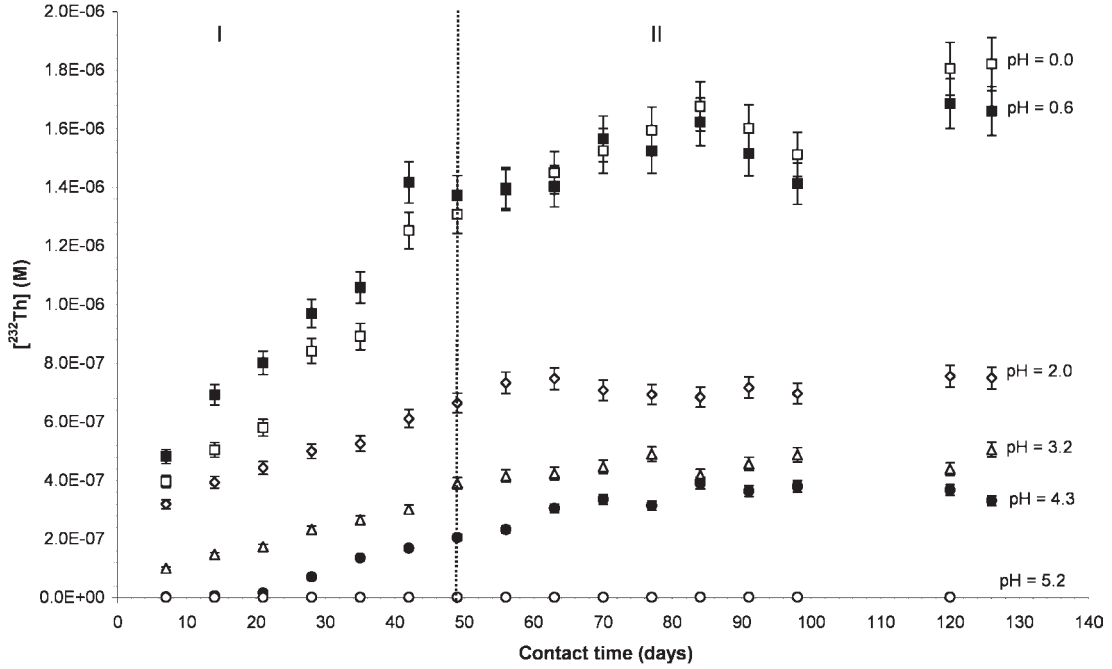

Figure 5. [^{232}Th] = *f*(contact time) for each pH value.

Table 7. Thorium Concentration Measured during Thorium Phase Dissolution and the NLR

	NLR ($g \cdot m^{-2} \cdot day^{-1}$)		
pH	NLR_I for $0 < t$ (days) < 50	NLR_{II} for $50 < t$ (days) < 130	[^{232}Th] ($mol \cdot L^{-1}$) for $t = 120$ days
0.0	7.65×10^{-4}	1.79×10^{-4}	1.81×10^{-6}
0.6	7.37×10^{-4}	0.98×10^{-4}	1.69×10^{-6}
2.0	2.62×10^{-4}	0.33×10^{-4}	7.56×10^{-7}
3.2	2.14×10^{-4}	0.26×10^{-4}	4.39×10^{-7}
4.3	1.75×10^{-4}	0.17×10^{-4}	3.68×10^{-7}
5.2	0.43×10^{-6}	0.29×10^{-6}	1.88×10^{-9}

surface regardless of the time of addition (at 0 or 133 days) and regardless of whether ^{232}Th dissolves fast or slow. Nevertheless, after 300 days, the [^{229}Th]$_{300}$ concentrations in series I experiments are in most cases about 2 times lower than those in series II experiments.

From the experimental data in Table 9, we see (1) that in all experiments the relative enrichment of ^{229}Th on the surface is $\gg 1$, (2) that the number of surface atoms of thorium participating in the exchange increases with decreasing pH, and (3) that the quantity of Th atoms participating in the exchange is higher when ^{229}Th spiking is performed at $t = 0$ days compared to spiking at $t = 130$ days.

5. Discussion

5.1. ThO_2(cr) Leaching Mechanism: Qualitative Side. We show in this study that our steady-state solution concentrations of thorium are much lower than most solubility data reported in the literature. This indicates that our system does not reach the thermodynamic solubility equilibrium. Consequently, the observed steady-state solution concentrations seem to be controlled kinetically. Moreover, when data[2] for a similar kind of solid (sintered ThO_2(cr), crystallized grains with grain boundaries) are compared to these data, we measure the same steady-state concentration but not the same normalized dissolution rate, NLR. We note that the surface is quite different and that the S/V ratio in our experiments is 2000 times lower than that in the previous study. In fact, the authors of the previous work[2] used a small grain size powder with many accessible grain boundaries. The powder was washed in strong acidic conditions, which probably removed all of the grain boundaries. This may be the reason why the leaching rate values of these authors[2] are much lower than those in our work. Also, in the case of these literature data, equilibrium was probably not obtained and solution concentrations appear to be controlled by kinetic constraints. On the other hand, the agreement between our solution concentrations and those of the authors does not allow any conclusion because in our solution concentrations appear to be controlled by the leaching of grain-boundary material, whereas in the other study,[2] they are controlled by matrix dissolution. Inversely, we can conclude a drop of 100−1000 times for the dissolution rates in the absence of grain boundaries in which leaching of Th(1) does not significantly contribute to the dissolution process observed in our case. Indeed, with the reported[1] ThO_2(cr) dissolution rate of 2×10^{-8} $g \cdot m^{-2} \cdot day^{-1}$ at pH 3.1, one would obtain for our experimental setup in 100 days only a concentration of 10^{-11} $mol \cdot L^{-1}$, much lower than was experimentally measured.

With the SEM and AFM pictures, we show two components at the surface: grains and grain-boundary matter assigned respectively to Th(1) = ThO_2(cr) and Th(2) = $ThO_x(OH)_y(H_2O)_z$(s) as identified by the XPS results, linking the OH and OH_2 components of the O_{1s} spectrum to the Th(2) site. The hydrated material may originate from the initial grain-boundary oxide materials, which are more reactive to humidity than bulk materials. Indeed, the OH_2 component has not been observed on the ThO_2(cr) sample studied here,[2] where grain boundaries have been washed off. This, and the mutual disappearance of Th(2) and the OH_2 component in the "leached pH 3.2" sample, shows

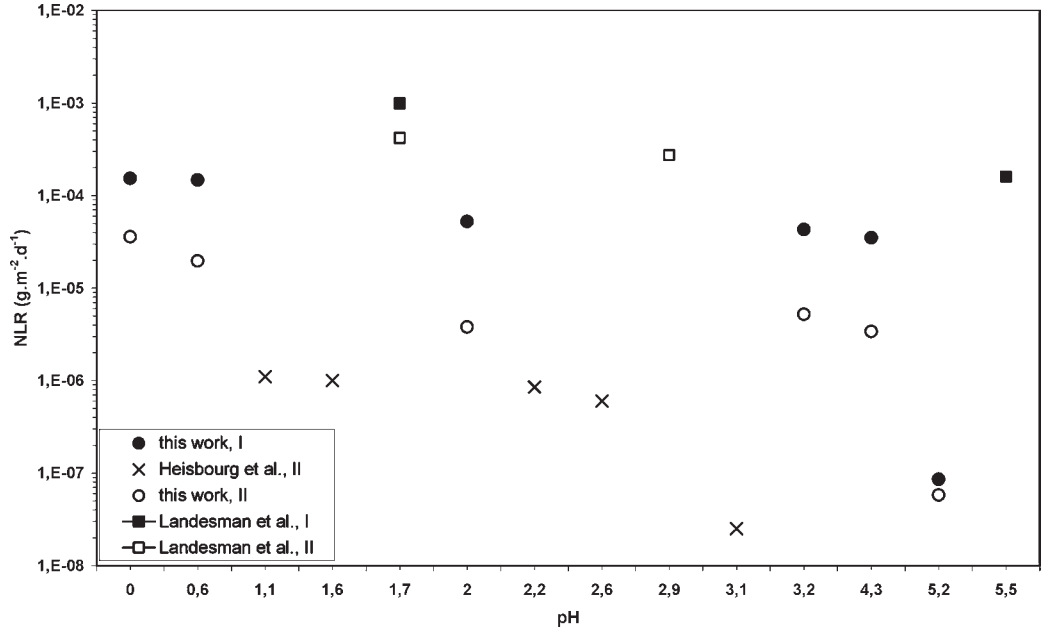

Figure 6. NLR = *f*(pH) for domain I (forward) and domain II (steady state) with data determined here.[1,2,6]

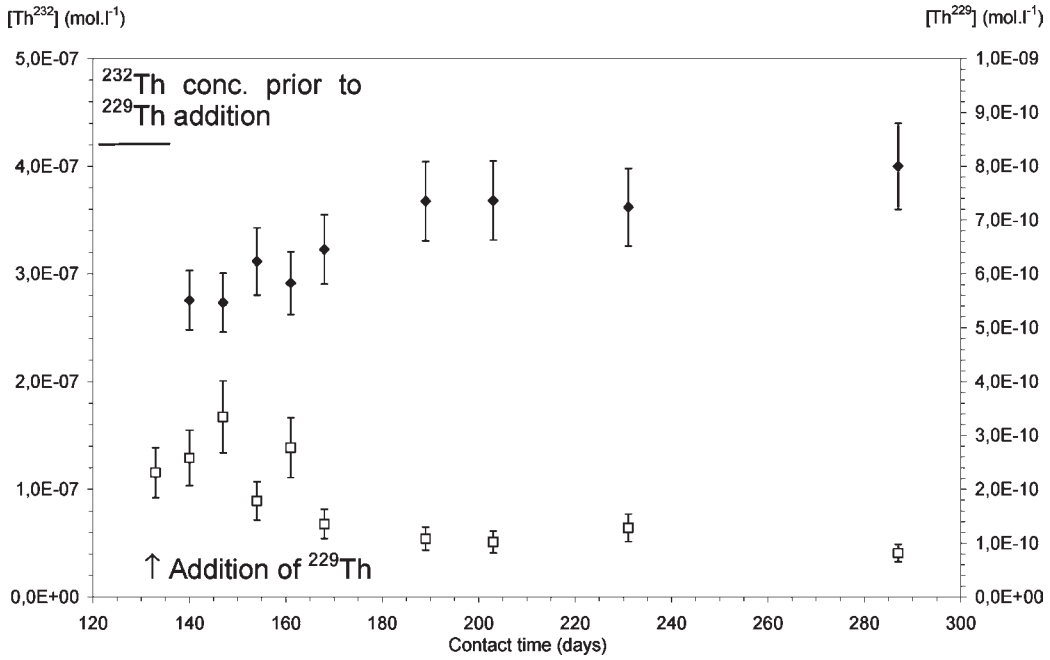

Figure 7. [^{232}Th] = *f*(time) (solid diamonds) and [^{229}Th = *f*(time) (open squares) for the 32-II experiment.

Table 8. [^{229}Th] Measured at t = 0, 133, and 300 days

sample	$[^{229}Th]_0$ (mol·L^{-1})	$[^{229}Th]_{133}$ (mol·L^{-1})	$[^{229}Th]_{300}$ (mol·L^{-1})
00-I	3.32×10^{-10}		0.44×10^{-10}
00-II		3.32×10^{-10}	0.82×10^{-10}
06-I	4.51×10^{-10}		1.00×10^{-10}
06-II		4.51×10^{-10}	2.04×10^{-10}
20-I	2.68×10^{-10}		0.70×10^{-10}
20-II		2.68×10^{-10}	1.25×10^{-10}
32-I	2.31×10^{-10}		0.25×10^{-10}
32-II		2.31×10^{-10}	0.81×10^{-10}

that molecular H_2O is associated with the Th(2) site. This hypothesis is additionally supported by an EXAFS study performed,[5] where the chemical environments of thorium in ThO_2(cr) and $ThO_x(OH)_y(H_2O)_z$(s) were described as quite different.

With the ^{232}Th/^{229}Th exchange experiments and considering the very low rate of Th(1) dissolution, we propose a leaching mechanism involving only the $ThO_x(OH)_y(H_2O)_z$ phase located in the grain boundaries, leaving the bulk grain matrixes less reactive. This explains the deepening of the grain boundaries observed by SEM and AFM. Moreover, during the leaching process, Th(2) surface sites are less and less accessible in the depth of the grain boundary, thus leading to a decrease of the dissolution rates with time. The decrease of the grain-boundary dissolution rates is so strong that it is interpreted as an approach to the "steady state" or of an apparent solubility

Table 9. Results of Dissolution and Isotopic Exchange Experiments with ThO_2

pH	^{229}Th addition at day	apparent "solubility" $[^{232}Th]$ $(mol \cdot L^{-1})$	$\frac{\left(\frac{^{229}Th}{^{232}Th}\right)_{surface}}{\left(\frac{^{229}Th}{^{232}Th}\right)_{solution}}$
0.0	0	1.81×10^{-6}	140
0.0	133		65
0.6	0	1.69×10^{-6}	70
0.6	133		24
2.0	0	7.56×10^{-7}	25
2.0	133		10
3.2	0	4.39×10^{-7}	43
3.2	133		10

equilibrium. Such a steady state would be reached after a time, which depends either on the accessibility of the $ThO_x(OH)_y(H_2O)_z$ phase located in grain boundaries or on the achievement of local chemical conditions in the grain boundaries, which slow down the dissolution rates. The observed solution concentrations of thorium at the end of the experiment, hence, are controlled by the quantity of leachable grain-boundary matter in the time of the experiment. Therefore, they are not related to thermodynamic equilibrium concentrations. Indeed, as was already observed, the time to reach solubility equilibrium for ThO_2(cr) is very long.[13] As mentioned above, the authors[13] explain the discrepancy in the thorium oxide/hydroxide solubility values with the difference in the particle size distribution. Our observations add another aspect to the overall picture of solubility control. We find that the accessibility of a $ThO_x(OH)_y(H_2O)_z$ phase located in limited amounts in the grain boundaries of ThO_2(cr) leads to low apparent solubility values. In contrast, free, accessible, fresh thorium hydroxide shows, as documented in the literature, much higher solubility values.

We have shown that one has also to consider the grain-boundary effect in addition to the discrepancy in the thorium oxide/hydroxide solubility data presented in Figure 1 caused by different particle size distributions.[13] In summary, the surface-sintered grain boundary rich in ThO_2(cr) is characterized by two sets of thorium oxide [ThO_2(cr) and $ThO_x(OH)_y(H_2O)_z$(s)], with the two surface sites Th(1) being less reactive and Th(2) being more reactive with respect to the leaching process. Certain generic lessons can be learned:

1 The ThO_2(cr) surface is mainly composed of grains of Th(1). In our case with sintered large spheres, these grains were surrounded by grain boundaries of Th(2). However, in many other solubility studies (see the review in ref 13), fine crystalline powders were used, where grain boundaries are either freely exposed or, as in the case of this study,[1,2] these grain boundaries are washed off by the initial sample treatment. The leaching is initially much faster in the cases in the presence of grain boundaries than in the cases with powdered material (see Figure 2), but the leaching rate decreases when Th(2) sites become less accessible. However, thermodynamic data cannot be obtained from our results: in the case of the coexistence of two phases related to Th(1) and Th(2), the thermodynamic solubility equilibrium is governed by the more soluble and more reactive phase. Hence, sintered ThO_2(cr) with grains and their grain boundaries cannot be used to measure the solubility of ThO_2(cr). Moreover, considering the constraints in the accessibility of grain boundaries, a "local solubility equilibrium" may be invoked in the grain boundaries (cf. Figure 8; see the discussion below).

2 For $ThO_x(OH)_y(H_2O)_z$(s), the surface is only composed of the Th(2) site. The solubility equilibrium is quickly reached at appropriate pH values. Authors[3] have shown that the solubility of $ThO_x(OH)_y(H_2O)_z$(s) decreases with respect to the heating time. This result may be explained by modification of the Th(2) site to the Th(1) site by the dehydration and crystallization processes. This crystallization phenomenon has already been reported[19] during oversaturated experiments.

5.2. Leaching Mechanism of Sintered Polycrystalline ThO_2(cr). A qualitative scheme of a leaching mechanism of our sample is proposed in Figure 8. Dissolution of the solid in the vicinity of the grain boundaries is controlled by two phenomena: (1) Diffusion of aqueous Th(aq) species from grain boundaries to the bulk solution driven by a gradient of Th(aq) concentrations. Similarly, there may be a pH gradient imposed by the pH change following the dissolution reaction in the grain boundary. In such a way, the system may maintain the local equilibrium conditions ($[Th]_{aq}$ and pH), which can be defined as a "local solubility equilibrium". (2) Water accessibility to the Th(2) sites in the grain boundaries. The Th(2) accessibility decreases with the leaching time. The sum of these processes may lead to a situation where the solubility equilibrium for the $ThO_x(OH)_y(H_2O)_z$(s) phase into the aqueous phase in grain boundaries is reached faster than that for ThO_2(cr) in a bulk solution.

We attempt to compare the experimental thorium concentrations measured in leaching solutions to those measured and/or calculated from the AFM and XPS results. Calculations for XPS and AFM data are detailed respectively in Appendices A and B in the Supporting Information. For this aim, we calculated the number of Th atoms at the solid surface from the thorium density in a unit cell (4 Th atoms per unit cell and $a = 5.5975$ Å[34]) and found a value of 1.1×10^{-5} mol·m^{-2}. For the XPS technique, the volume analyzed is a 150-μm-diameter spot with a depth of 3 nm. The very low depth of analysis is the reason why the Th(2) contribution is no longer observed after the leaching process. In fact, AFM results show that the leaching process reaches down to a depth of 50 nm. Moreover, we use the ratio of 81/19% for Th(1)/Th(2) measured by XPS. Table 10 presents the results of the thorium solution concentration calculated by the mass balance and geometric constraints from XPS data. Hence, for the overall solid surface in contact with the solution, the calculated concentration is $[Th]_{aq} = 1.7 \times 10^{-7}$ mol·L^{-1}. This value is on the same order of magnitude as the thorium concentration in solution measured by ICP-MS (4.4×10^{-7} mol·L^{-1} for the sample leached at pH 3.2).

(34) Cohen, I.; Berman, R. M., A metallographic and X-ray study of the limits of oxygen solubility in the UO_2-ThO_2 system. *J. Nucl. Mater.* **1966**, *18*, (2), 77-107.

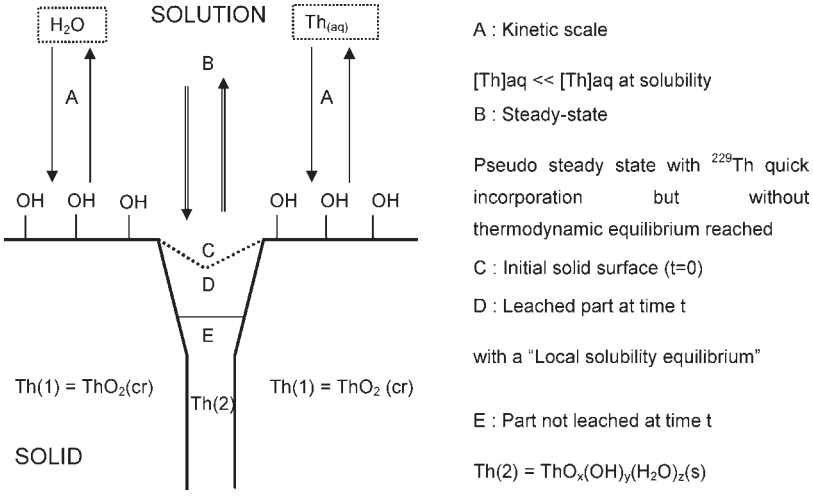

Figure 8. ThO_2 sphere leaching mechanism.

Table 10. XPS Data Used To Calculate the Released Thorium Concentration for the "Leached pH 3.2" Sample (Appendix A in the Supporting Information)

analysis area		solid studied		$[Th]_{aq}$ released	
xy size	150 μm	unit cell volume	1.75×10^{-28} m^3	for the surface analyzed	2.5×10^{11} mol·L^{-1}
z size (depth)	3 nm	number of Th atoms analyzed	1.21×10^{12}	for the total surface	1.7×10^{-7} mol·L^{-1}
volume analyzed	5.30×10^{-17} m^3	Th(1) = 81%	9.8×10^{11}		
		Th(2) = 19%	2.3×10^{11}		

Table 11. AFM Data Used To Calculate the Released Thorium Concentration for the "Leached pH = 3.2 Sample" (Appendix B in the Supporting Information)

grain		solid in solution		$[Th]_{aq}$ released
average size	1 μm	surface	1.2×10^{-4} m^2	1.8×10^{-8} mol·L^{-1}
perimeter	3.14×10^{-6} m	number of grains	1.5279×10^{8}	
depth leached	50 nm	[Th] at the surface	1.1×10^{-5} mol·m^{-2}	

Using the leaching depth and the grain size in the *x*, *y*, and *z* directions (1 μm for the *xy* size and 300 nm for the *z* size) derived from AFM data, we also calculate the thorium concentration in the aqueous solution for the leaching experiments. Table 11 presents results obtained from the AFM data. The results give 1.8×10^{-8} mol·L^{-1}, about 25 times lower than the experimental value for pH 3.2 (4.4×10^{-7} mol·L^{-1}).

With these data derived from solid analysis (cf. Table 12), we can propose a quantification of the leaching process onto the grain boundaries of the ThO_2(cr) studied here. Calculations are presented in Appendix C in the Supporting Information. Concerning the AFM measurements, the ratio between the measured and calculated thorium concentrations in solution leads us to the conclusion that an average grain-boundary thickness of 25 monolayers (about 12 nm) is dissolved in the leaching process over a depth of 50 nm. Concerning XPS data, if we take into account the analyzed volume (Table 10 and Annex A), 85 monolayers are calculated to be involved during the leaching process at the solid surface. Hence, quantification of the leached surface is possible and consistent with the quantity of thorium measured in solution.

5.3. Leaching Mechanism of Sintered Polycrystalline ThO_2(cr): Spiking ^{229}Th Contribution. We conclude from the above observations (1) that the apparent solubility values measured are not controlled by the ThO_2 grains and (2) that the measured solubility is probably determined by the kinetics of release of amorphous or nanocrystalline grain-boundary material. Our experiments using isotopic species allow one to assess the reversibility of the involved reaction system.

If there is complete reversibility (isotopic equilibrium) for the isotopic tracer, the isotopic ratios on the surface divided by those in solution must remain unchanged during the experiment. This must also be independent of the time of the addition of the tracer. Consequently, the observed increase in ^{229}Th surface uptake (Table 9) for the addition of the tracer at $t = 0$ day when compared to the addition at $t = 133$ days indicates irreversible fixation of the tracer isotope on the surface. Thus, the irreversibility is due to a means incorporation of ^{229}Th on the surface or subsurface structure of the solid. Because solid-state diffusion is very slow, it cannot explain the irreversible trapping of ^{229}Th by this mechanism. Alternatively, one may invoke, as an explanation, either precipitation of some atomic layers on the existing solid or precipitation of a new phase. There may be also surface incorporation of ^{229}Th when ^{229}Th is added after 133 days. It could as well be that the large surface uptake is not due to the irreversible trapping but to a much higher reactive surface area of the grain-boundary material as opposed to the geometric surface area, which was used to calculate isotopic enrichment at the surface. Hence, from the difference in the ^{229}Th uptake between the two additions at either 0 or 133 days, one may estimate the minimum amount of precipitated solid phase assuming no additional precipitation after 133 days. This difference is about 15−75 times higher than the thorium content of a monolayer. Additionally, on the basis of the known

Table 12. Data Used for Quantification of the Grain-Boundary Leaching Process (Appendix C in the Supporting Information)

AFM		XPS	
[Th] calculated for 1 monolayer	1.8×10^{-8} mol·L^{-1}	Th(2) volume analyzed	1.01×10^{-17} m^3
		surface leached	2.12×10^{-10} m^2
[Th] experimental	4.4×10^{-7} mol·L^{-1}	depth leached	47.6 nm
		one monolayer z size	0.56 nm
number of monolayers	25	number of monolayers	85

thermodynamics of thorium, it is impossible between pH 0 and 2 to encounter in bulk solution precipitation of either a crystalline or an amorphous phase under our experimental conditions if bulk solution concentrations of thorium are lower than 10^{-6} mol·L^{-1}. The observed precipitation and irreversible isotopic uptake can, therefore, only be explained if, at some place in the reaction system, the local pH is much higher than the bulk pH. This phenomenon does not occur at the surface of ThO_2-(cr) because this is easily accessible and does not allow the establishment of a strong pH gradient. The only place where access is difficult is the grain boundaries; therefore, a pH gradient is not expected to occur there. This is consistent with the vision that the principal site for dissolution is the grain boundary because the dissolution reaction consumes protons. We conclude that both dissolution and precipitation occur sufficiently deep in grain boundaries and are not measurable by XPS.

Considering that the initial grain-boundary material occupies about 20% of the geometric surface (observation from XPS and AFM), the precipitated material corresponds to at least 75−375 monolayers [(15−75)/0.2] or 4−20 nm. This corresponds to a single spherical particle of 7−35 ng for ThO_2 (calculated from the relative cross-sectional area of grain boundary = 0.2 × total surface, thickness, and density).

From the isotopic uptake at 133 days, we can deduce that no further precipitation occurs and that the surface of reversible exchange is between 10 and 65 times as high as the geometric surface area of the sphere, considering that this exchange occurs reversibly either on the remaining grain-boundary material or on the precipitated material. Hence, reversible exchange also occurs on the grain boundary. We can in this way determine the specific surface area of the precipitate as 1200−1600 m^2·g^{-1}. This very high specific surface area clearly demonstrates the amorphous character of the precipitate.

We have thus three phases in our system: ThO_2(cr), the initial grain-boundary material, which has dissolved at least partly, and a precipitated material. There is no way to prove that the dissolved grain-boundary material is more similar in structure than the precipitated phase. From the assumed reversibility at the surface of the precipitate, one can conclude that this phase controls the observed apparent solubility. Considering the abovementioned pH gradients between the interior of the grain boundary and the bulk solution, we conclude that the measured solubility does not correspond to the solubility of the precipitate in a bulk solution at bulk pH but to that for the pH in the aqueous phase in the grain boundary. From the literature data on the solubility of amorphous $Th(OH)_4$ in a bulk solution as a function of the pH and from the measured solubility, we can estimate the grain-boundary pH: for a bulk solution with a pH of 0−0.6, we obtain a grain-boundary pH of about 5; for a bulk pH of 2−3.2, we have a grain-boundary pH of about 5.3. The pH increase is a direct consequence of eq 1 at very high S/V values operative within the grain-boundary pore water.

6. Conclusion

This study gives some insights on the oxide/hydroxide thorium solubility and we list these below.

i The surface of sintered multigrain ThO_2(cr) is characterized by bulk ThO_2(cr) grains (80%) surrounded by $ThO_x(OH)_y(H_2O)_z$(s) grain boundaries (20%). The hydrated material may originate from the initial grain-boundary oxide materials, which are more reactive to humidity than the bulk materials. The solubility of these two phases is quite different. It is lower for the ThO_2(cr) phase and higher for the $ThO_x(OH)_y(H_2O)_z$(s) one. We provide evidence that the leaching process mainly occurs in the grain-boundary space rather than on the grain surfaces.

ii The ^{229}Th spiking experiments show the phenomenon of dynamic dissolution/precipitation reactions at the solid/solution interface. Irreversible isotopic uptake (local precipitation in grain boundaries) is observed under conditions where the global dissolution reaction is still ongoing.

iii Our work adds another aspect to the understanding of the large discrepancies in thorium solubility data described in the literature: not only are they due to the variety of different thorium phases used in these studies, with different particle sizes (as described in ref 13), but a single sample may be characterized by the coexistence of various phases (in our case, the crystalline bulk solid, an amorphous grain-boundary phase, and a phase precipitated in grain boundaries) and that apparent solubility is linked to reactive phase accessibility.

iv Moreover, a "local solubility" occurs at the grain boundaries providing the most active sites. This "local solubility" is constrained by local conditions such as the pH and thorium concentration in solution located in the grain boundaries. The gradient of the parameters between grain boundaries and the bulk solution controls the solubility measurements performed in this study and may be as well in previous studies.

In conclusion, the thermodynamic equilibrium concept of solubility cannot be strictly applied to certain types of solids with a particular chemical composition. Detailed surface characterization and assessment of the reversibility by isotopic techniques is a prerequisite to better describe the solubility in aqueous solutions. The bulk solubility of solids just reflects an average of the localized solubility depending on the amount of reactive surface sites. A deeper and more

accurate characterization of the solid surface heterogeneity is then required to better study their solubility.

Acknowledgment. The authors acknowledge financial support by the French Agence Nationale de Recherche, ANR, in Project SOLRAD. We acknowledge V. Fernandez from the IMN and J. P. Guin from LARMAUR for letting us perform XPS and AFM measurements, K. Perrigaud from SUBATECH for ICP-MS analyses of dissolved ^{232}Th, and J. Neeway for reviewing the paper.

Supporting Information Available: Calculations from XPS and AFM data and those to determine the thickness of leached monolayers. This material is available free of charge via the Internet at http://pubs.acs.org.